Journal of Materials Chemistry C

PAPER

View Article Online
View Journal | View Issue

Cite this: J. Mater. Chem. C, 2014, 2, 4027

Bent-rod liquid crystal dimers: synthesis and mesomorphic properties

Nerea Sebastián,[a] Nélida Gimeno,[b] Jorge Vergara,[b] David O. López,[c] José Luis Serrano,[d] César L. Folcia,[e] M. Rosario de la Fuente*[a] and M. Blanca Ros*[b]

Received 31st January 2014
Accepted 11th March 2014

DOI: 10.1039/c4tc00212a

www.rsc.org/MaterialsC

The synthesis and characterization of three bent-rod dimers are reported. Very long flexible spacers that include methylene units and either a phenyl ring or a triazole moiety as connecting structures join the bent- and rod-promesogenic cores. Polarizing microscopy, modulated differential scanning calorimetry, X-ray diffraction at variable temperature and dielectric measurements have been performed to establish the mesophase behaviour of the dimers. The results show a complex supramolecular organization for this kind of flexible dimer in the mesophase. Interestingly, the length and the chemical nature of the flexible linking spacers condition the liquid crystalline properties of these novel compounds. Additionally, it has been found that the chemical structure of the rod-like core plays a key role in determining the kind of mesophase, either nematic or lamellar, formed by these materials.

Introduction

Liquid crystalline dimers consist of two mesogenic units connected by a flexible spacer. These mesogenic molecules have attracted a great deal of interest in liquid crystal research for two main reasons. On the one hand, these materials can be considered as model compounds for higher molecular weight structures such as main-chain and side-chain polymers. On the other hand, these materials have become more appealing as they have proven to show complex and novel mesomorphism that is markedly different from that of the corresponding monomers.[1,2] In particular, some odd rod-like cyanobiphenyl dimers exhibit a new twist-bent nematic phase.[1e,f] Research into mesogenic dimers has been mainly focused on the combination of rod-like calamitic units of equal or different nature (polar, non-polar, chiral, and non-chiral).[1] Non-symmetric dimers that combine rod- and disc-like mesogens or symmetric dimers that contain two discotic units have been studied to a lesser extent.[2]

The discovery of a new type of liquid crystal, the so-called bent-core liquid crystals (BCLCs), by Niori *et al.* in 1996[3] opened up new possibilities in dimer research. BCLCs have been the focus of extensive research due to the novel and extraordinary properties shown by the mesophases of these materials.[4] The ability of these materials to form polar order and phase chirality without the molecules being chiral along with their interesting properties (such as ferro-, antiferro- and piezoelectricity, nonlinear optical activity, and high flexoelectric behaviour) have stimulated the research in this field.[5] Moreover, the biaxial molecular shape of these materials makes them good candidates to present thermotropic biaxial nematic phases.[6] The search for biaxiality in BCLCs has been split into two main areas: the bent-shaped molecules themselves and their linear covalent coupling with a rod-like unit to form a nonsymmetrical dimer in order to enhance the shape biaxiality of the rod-like mesogen.[7] Of these approaches, the research into hybrid rod-like and bent-core liquid crystalline dimers to give biaxial phases has attracted the most attention. Yelamaggad *et al.*[8] reported an N_b-SmA_b sequence in a dimer that combines a bent-core unit and a rod-like cyanobiphenyl derivative linked by a hexamethylene spacer. In this first example, the crucial role of the parity of the spacer was highlighted, as the same dimer with an odd spacer was not mesomorphous. This effect is also appealing in dimers derived from calamitic units. The same odd–even effect and the N-SmA phase sequence have also been described for a different series of bent-core/cyanobiphenyl dimers by Lee *et al.*[9] More recently, Li *et al.*[10] have found the same type of sequence in substituted bent-core mesogens linked by hexamethylene spacers to cyanobiphenyl units. However, biaxiality could be only confirmed for the SmA phase. Other interesting phase sequences have been achieved by the combination of bent-core and rod-like structures within the same molecule. By modulating the parity of the methylene

[a]Departamento de Física Aplicada II, Facultad de Ciencia y Tecnología, Universidad del País Vasco UPV/EHU, Apdo. 644, 48080-Bilbao, Spain. E-mail: rosario.delafuente@ehu.es

[b]Instituto de Ciencia de Materiales de Aragón, Universidad de Zaragoza-CSIC, Departamento de Química Orgánica, Facultad de Ciencias, Pedro Cerbuna, 12, 50009 Zaragoza, Spain. E-mail: bros@unizar.es

[c]Grup de Propietas Físiques dels Materials (GRPFM), Departament de Física i Enginyeria Nuclear, E.T.S.E.I.B. Universitat Politècnica de Catalunya, Diagonal, 647 08028 Barcelona, Spain

[d]Instituto de Nanociencia de Aragón, Universidad de Zaragoza, Departamento de Química Orgánica, Facultad de Ciencias, Pedro Cerbuna 12, 50009-Zaragoza, Spain

[e]Departamento de Física de la Materia Condensada, Facultad de Ciencia y Tecnología, Universidad del País Vasco UPV/EHU, Apdo. 644, 48080-Bilbao, Spain

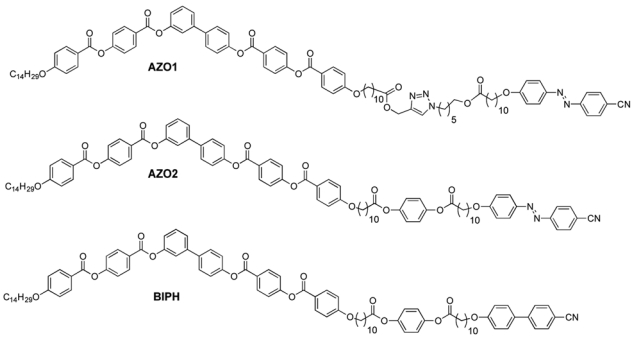

Scheme 1 Chemical structures of the bent-core and rod-core based dimers: AZO1, AZO2 and BIPH.

linker, blue phases and columnar phases have been obtained by Yelamaggad *et al.* for non-symmetric dimers in which bent-core units are combined with a cholesterol derivative.[11] Furthermore, azobenzene-derived calamitic units have also been coupled with bent-core units in order to achieve photoreactive dimers.[12] Thus, besides the type and size of mesogenic units, the parity and nature of the spacer have proven to be crucial in the properties of the dimeric systems.[13]

Herein we report the synthesis and broad characterization of three new non-symmetric dimers denoted as **AZO1**, **AZO2** and **BIPH**. These compounds contain the same six-ring bent-core structure and two different rod-like moieties derived from azobenzene (AZO) and cyanobiphenyl (BIPH) (see Scheme 1).

Previous reports have focused on bent-rod dimers that connect the promesogenic units by a relatively short linear spacer (from 3 to 10 methylene units). In contrast, with the aim of studying the effect of the promesogenic core decoupling on the supramolecular organization of this type of bent-rod dimer, we selected a very long and flexible connection between the promesogenic structures. This assembly consists of two long spacers linked either by a phenyl ring or a more flexible hexamethylene-triazole moiety. It will be shown that the role of this part of the dimer is crucial for the mesomorphism, with two out of the three dimers being mesomorphous. Furthermore, appropriate selection of the rod-like core can be used to tune the liquid crystal organization of the dimer. A detailed thermal, structural and dielectric study of these compounds has been carried out and the results reveal a rich and complex behaviour.

This paper has been structured as follows. The experimental details are described in the first section. The liquid crystalline properties (studied by microscopy, X-ray diffraction and modulated differential scanning calorimetry) and dielectric characterization are presented in the second section and, finally, the concluding remarks are covered.

Experimental section

1. Synthesis of compounds

The synthetic routes followed to prepare the three dimers are shown in Schemes 2–4. All of the bent-rod dimers synthesized are based on the same six-ring bent-shaped structure derived from 3,4′-biphenyl, which has a well-documented ability to induce BCLC phases.[5c,14] The preparation of bent-core and rod-like intermediates, alkyne **3** (ref. 14) and acids **4**,[14] **1** and **8** has been described previously.[15]

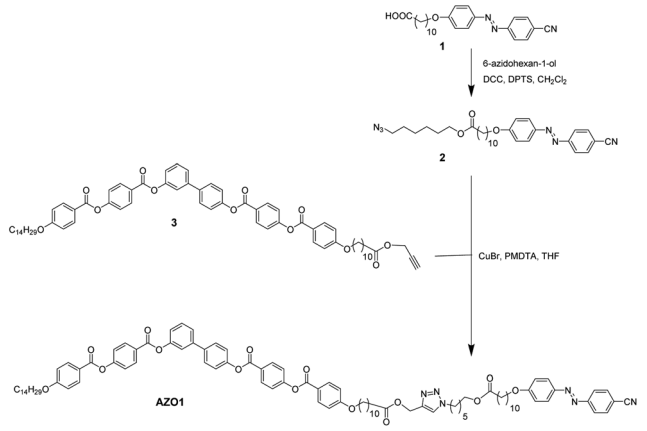

Scheme 2 Synthetic route followed to synthesize dimer AZO1.

The promesogenic unit of compound **2** was prepared by esterification of acid **1** with 6-azidohexan-1-ol. The product was then coupled with alkyne **3** using standard 'click chemistry' conditions to obtain dimer **AZO1** (see Scheme 2). The dimer **AZO2** was synthesized by esterification of the bent-shaped acid **4** with trimethylsilyl monoprotected hydroquinone to give compound **5**, which was deprotected and reacted with rod-shaped acid **1** under Steglich conditions to yield the final product (Scheme 3). An analogous sequence of reactions was followed for the preparation of dimer **BIPH**, but in this case the rod-like acid **8** was first esterified with trimethylsilyl monoprotected hydroquinone to obtain compound **9**. Deprotection of

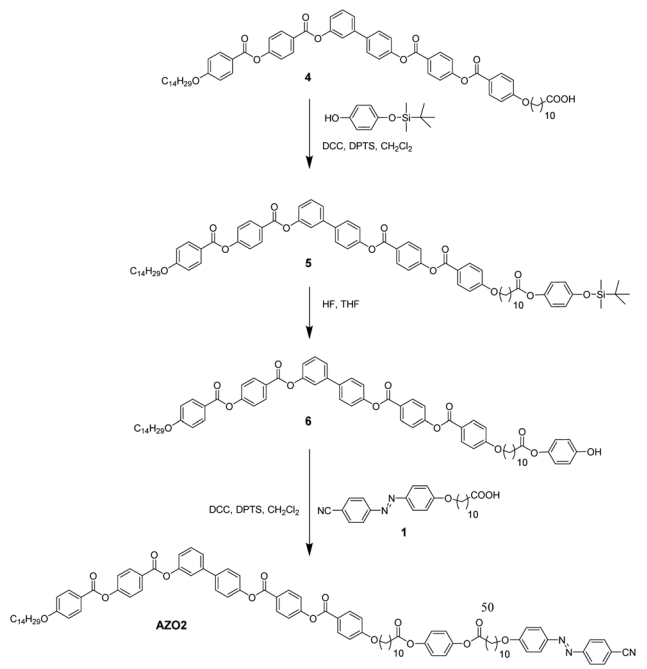

Scheme 3 Synthetic route followed to synthesize dimer AZO2.

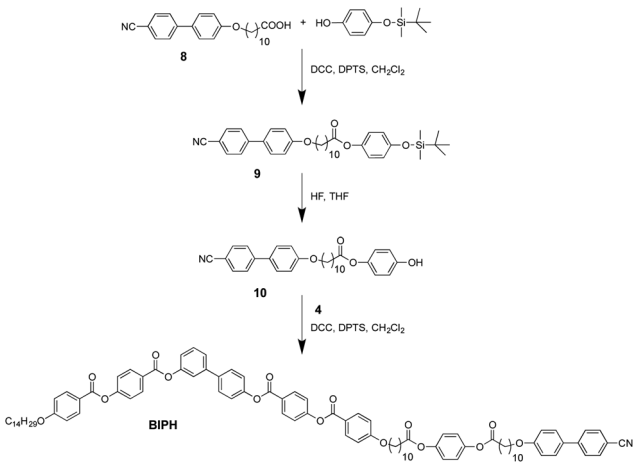

Scheme 4 Synthetic route followed to synthesize dimer **BIPH**.

this compound yielded phenol **10** and this was esterified with bent-core compound **4** to yield the pure dimer **BIPH** (Scheme 4).

Details of the synthesis and full characterization data for all compounds are given below.

Compound 2. Acid **1** (0.50 g, 1.22 mmol), DPTS (0.36 g, 1.22 mmol), DCC (0.35 g, 1.7 mmol) and 6-azidohexan-1-ol (0.50 g, 1.22 mmol) were stirred in dry dichloromethane (30 mL) for 24 h. The crude product was purified by liquid chromatography on silica gel using dichloromethane as eluent. Compound **2** was obtained as an orange solid. Yield: 0.36 g (53%). M.p. (°C): 73. ^{1}H NMR (400 MHz, $CDCl_3$) δ (ppm) = 1.30–1.38 (m, 16H), 1.60 (m, 6H), 1.81 (m, 2H), 2.29 (t, J = 7.4 Hz, 2H), 3.26 (t, J = 6.8 Hz, 2H), 4.06 (t, J = 6.5 Hz, 4H), 7.00 (d, J = 8.9 Hz, 2H), 7.76 (d, J = 8.4 Hz, 2H), 7.92 (d, J = 8.8 Hz, 4H). ^{13}C NMR (100 MHz, $CDCl_3$) δ (ppm) = 25.0, 25.6, 26.0, 26.4, 28.5, 28.8, 29.1, 29.3, 29.4, 29.5, 34.4, 51.3, 64.1, 68.5, 113.1, 114.9, 123.1, 125.5, 133.2, 146.7, 154.8, 162.8, 174.9. FTIR (KBr, ν cm^{-1}): 2915, 2854, 2230, 2104, 1721, 1595, 1572, 1268. MALDI-MS m/z = 555.3 $[M + Na]^+$.

Compound AZO1. Compound **3** (0.15 g, 0.14 mmol), compound **2** (0.08 g, 0.15 mmol) and CuBr (0.04 g, 0.28 mmol) were placed in a dry Schlenk tube. Three vacuum/argon cycles were performed and dry and degassed THF (3 mL) and PMDETA (58 μL, 0.28 mmol) were added. Three freeze–thaw cycles were carried out and the mixture was stirred at room temperature for 24 h. The mixture was filtered through neutral alumina and the solvent was evaporated. The crude product was purified by column chromatography using dichloromethane–ethyl acetate (7/3) as eluent. The pure product was dissolved in the minimum amount of dichloromethane and precipitated from hexanes. Yield: 0.12 g of an orange solid (55%). M.p. (°C): 108. ^{1}H NMR (300 MHz, $CDCl_3$) δ (ppm) = 0.88 (t, J = 6.5 Hz, 3H), 1.28–1.47 (m, 48H), 1.61–1.64 (m, 6H), 1.81–1.93 (m, 10H), 2.27–2.36 (m, 4H), 4.04 (m, 8H), 4.34 (t, J = 7.2 Hz, 2H), 5.21 (s, 2H), 6.98–7.04 (m, 6H), 7.20–7.23 (m, 1H), 7.32 (d, J = 8.5 Hz, 2H), 7.40 (d, J = 8.8 Hz, 4H), 7.47 (s, 1H), 7.52 (d, J = 4.8 Hz, 2H), 7.60 (s, 1H), 7.68 (d, J = 8.6 Hz, 2H), 7.79 (d, J = 8.5 Hz, 2H), 7.94 (d, J = 8.7 Hz, 4H), 8.17 (d, J = 8.5 Hz, 4H), 8.33 (dd, J = 2.9 Hz, J = 8.8 Hz, 4H). ^{13}C NMR (75 MHz, $CDCl_3$) δ (ppm) = 14.1, 17.8, 22.7, 24.8, 24.9, 25.3, 26.0, 26.1, 28.3, 29.1, 29.2, 29.3, 29.4, 29.5, 29.6, 30.1, 31.9, 34.1, 34.3, 46.3, 50.2, 57.4, 64.8, 65.2, 68.3, 68.4, 68.5, 113.1, 114.4, 114.8, 118.6, 120.4, 120.9, 122.0, 122.1, 123.0, 124.7, 125.4, 126.8, 128.3, 129.9, 131.8, 132.4, 133.1, 138.0, 142.0, 150.6, 151.3, 155.4, 162.7, 163.8, 164.3, 164.4, 164.5, 172.3, 173.2, 173.7. FTIR (KBr, ν cm^{-1}): 2926, 2849, 2213, 1726, 1595, 1501, 1260. MALDI-MS m/z = 1640.9 $[M + Na]^+$. EA for $C_{98}H_{116}N_6O_{15}$: calc.: C 72.74, H 7.23, N 5.20; found: C 72.58, H 7.25, N 5.20%.

Compound 5. Acid **4** (0.30 g, 0.30 mmol), DPTS (0.84 g, 0.30 mmol), DCC (0.84 g, 0.40 mmol) and 4-*tert*-butyldimethylsilyloxyphenol[15a] (0.64 g, 0.30 mmol) were stirred in dry dichloromethane (50 mL) for 24 h. The crude product was purified by liquid chromatography on silica gel using dichloromethane–ethyl acetate (10 : 0.2) as eluent. Compound **5** was obtained as a white solid. Yield: 0.31 g (87%). M.p. (°C): 70. ^{1}H NMR (400 MHz, $CDCl_3$): δ (ppm) = 0.20 (s, 6H, CH_3), 0.88 (t, J = 6.6 Hz, 3H, –CH_3), 0.99 (s, 9H, CH_3), 1.27 (m, 34H), 1.84 (m, 6H), 2.54 (t, J = 7.3 Hz, 2H, H_2C═O), 4.07 (t, J = 6.0 Hz, 4H, –CH_2O), 6.80 (d, J = 8.5 Hz, 2H), 7.93 (d, J = 8.5 Hz, 2H), 6.99 (d, J = 8.4 Hz, 4H), 7.27 (m, 1H), 7.31 (d, J = 8.2 Hz, 2H), 7.41 (d, J = 8.0 Hz, 4H), 7.47 (m, 1H), 7.52 (d, J = 4.7 Hz, 2H), 7.70 (d, J = 8.1 Hz, 2H), 8.16 (d, J = 8.8 Hz, 4H), 8.30 (d, J = 8.8 Hz, 4H). ^{13}C NMR (100 MHz, $CDCl_3$) δ (ppm) = −6.1, 14.1, 22.7, 24.9, 25.6, 26.0, 29.1, 29.3, 29.4, 29.5, 29.6, 29.7, 31.9, 34.3, 68.4, 114.4, 120.5, 120.9, 122.1, 122.2, 122.3, 124.7, 126.8, 126.9, 128.3, 131.8, 132.4, 138.0, 142.1, 151.3, 155.4, 163.8, 164.3, 164.5. FTIR (KBr, ν cm^{-1}): 2926, 2848, 1735, 1610, 1486, 1252. MALDI-MS m/z = 1275.7 $[M + Na]^+$.

Compound 6. Compound **5** (0.26 g, 0.2 mmol) was dissolved in THF (15 mL) in a plastic vessel. Hydrofluoric acid (150 μL, 49% aqueous solution) was added by syringe and stirred. The reaction was diluted with dichloromethane and quenched with a saturated solution of sodium bicarbonate. The resultant mixture was washed several times with water and the crude product was purified by column chromatography using dichloromethane–ethyl acetate (10/0.2) as eluent. Yield: 0.16 g of a white solid (68%). M.p. (°C): 147. ^{1}H NMR (400 MHz, $CDCl_3$): δ (ppm) = 0.88 (t, J = 6.9 Hz, 3H), 1.27–148 (m, 34H), 1.74 (m, 2H), 1.83 (m, 4H), 2.53 (t, J = 7.4 Hz, 2H), 4.06 (t, J = 6.4 Hz, 4H), 5.07 (s, 1H), 6.79 (d, J = 8.8 Hz, 2H), 6.91 (d, J = 8.8 Hz, 2H), 6.98 (d, J = 8.7 Hz, 4H), 7.23 (m, 1H), 7.31 (d, J = 8.6 Hz, 2H), 7.40 (d, J = 8.7 Hz, 4H), 7.46 (m, 1H), 7.52 (d, J = 4.8 Hz, 2H), 7.66 (d, J = 8.6 Hz, 2H), 8.15 (d, J = 8.6 Hz, 4H), 8.29 (d, J = 8.5 Hz, 2H), 8.32 (d, J = 8.6 Hz, 2H). ^{13}C NMR (100 MHz, $CDCl_3$): δ (ppm) = 14.3, 22.6, 24.7, 25.8, 26.4, 29.2, 29.3, 29.4, 29.5, 29.6, 29.7, 31.8, 34.7, 68.4, 114.4, 120.5, 121.0, 122.1, 122.2, 122.6, 124.7, 126.8, 127.0, 128.3, 131.8, 132.4, 138.2, 142.1, 151.4, 155.4, 163.8, 164.3, 165.5. FTIR (KBr, ν cm^{-1}): 3200, 2920, 2848, 1738, 1605, 1540, 1251. MALDI-MS m/z = 1161.6 $[M + Na]^+$.

Compound AZO2. Acid **1** (0.05 mg, 0.12 mmol), DPTS (0.04 mg, 0.12 mmol), DCC (0.04 mg, 0.17 mmol) and compound **6** (0.14 g, 0.12 mmol) were stirred in dry dichloromethane (20 mL) for 24 h. The crude product was purified by liquid chromatography on silica gel using dichloromethane–ethyl acetate (10 : 0.2) as eluent. Compound **AZO2** was obtained as an orange solid. Yield: 0.12 g (64%). M.p. (°C): see Table 1. H NMR (400 MHz, $CDCl_3$): δ (ppm) = 0.89 (t, J = 6.6 Hz, 3H, –CH_3), 1.27–1.49 (m, 48H), 1.83 (m, 8H), 2.55 (t, J = 7.3 Hz, 4H), 4.06 (t, J = 6.5 Hz,

Table 1 Transition temperatures (°C) and enthalpies (ΔH, kJ mol^{-1}) determined by DSC and MDSC for dimers **AZO1**, **AZO2** and **BIPH**

Compound	Phase transition temperature [°C] and enthalpy[a] [kJ mol^{-1}]
AZO1[b]	Cr 108 [103.3] I
AZO2[c]	Cr 119.7 [76.9[d]] M 125.5[e] [0.26[e]] N 140.2 [0.59] II 140 N 123 M 120 Cr
BIPH[c]	SmY glassy 45 SmY 128.2 [45.5[f]] SmX-N 135[g] [0.5[g]] II 137 N-SmX 125 SmY 49 SmY glassy

[a] Cr: crystal, N: nematic mesophase, M: unidentified mesophase, SmX, SmY: lamellar mesophases, SmY glassy: SmY vitrified phase, and I: isotropic liquid. [b] Data obtained by means of standard DSC measurements at 10 K min^{-1}. [c] Data obtained by means of MDSC measurements at 1 K min^{-1}. [d] Heat capacity peak attributed to the Cr-to-M-to-N phase transition. Enthalpy value corresponds to the set of both transitions and is overestimated for the single Cr-to-M phase transition. [e] Temperature and enthalpy data correspond to heating runs from 120 °C after a slow cooling from the isotropic phase. [f] Inferred by subtracting the enthalpy of the isolated N-to-I phase transition from the value measured for the SmY-to-(SmX + N) phase transition. [g] Obtained from the isolated N-to-I phase transition, measured at a rate of 0.5 K min^{-1} after slow cooling from the isotropic phase.

6H), 6.98 (m, 6H), 7.09 (s, 4H), 7.23 (m, 1H), 7.32 (d, J = 8.6 Hz, 2H), 7.38 (d, J = 8.8 Hz, 4H), 7.47 (m, 1H), 7.53 (d, J = 4.9 Hz, 2H), 7.67 (d, J = 8.6 Hz, 2H), 7.78 (d, J = 8.6 Hz, 2H), 7.94 (d, J = 8.7 Hz, 4H), 8.16 (d, J = 8.67 Hz, 4H), 8.29 (d, J = 8.7 Hz, 2H), 8.32 (d, J = 8.7 Hz, 2H). ^{13}C NMR (100 MHz, $CDCl_3$): δ (ppm) = 14.1, 22.7, 24.8, 15.9, 19.0, 29.2, 29.3, 29.4, 29.5, 29.6, 31.9, 34.3, 68.3, 68.4, 113.1, 114.4, 114.8, 120.4, 120.9, 122.1, 122.4, 123.0, 124.7, 125.4, 126.8, 128.3, 129.9, 131.8, 132.4, 133.1, 138.0, 142.0, 146.6, 147.9, 148.0, 150.6, 151.3, 154.8, 155.4, 162.7, 163.8, 164.3, 164.4, 172.2. FTIR (KBr, ν cm^{-1}): 2938, 2842, 2224, 1736, 1650, 1504, 1242. MALDI-MS m/z = 1551.7 $[M + Na]^+$. EA for $C_{95}H_{105}N_3O_{15}$: calc.: C 74.63, H 6.92, N 2.75; found: C 74.71, H 6.90, N 2.92%.

Compound 9. Rod-shaped acid **8** (1.00 g, 2.6 mmol), DPTS (0.80 g, 2.6 mmol), DCC (0.80 g, 3.9 mmol) and 4-*tert*-butyldimethylsilyloxyphenol (0.60 g, 0.26 mmol) were stirred in dry dichloromethane (50 mL) for 24 h. The crude product was purified by liquid chromatography on silica gel using dichloromethane as eluent. Compound **9** was obtained as a white solid. Yield: 1.47 g (95%). M.p. (°C): 70. ^{1}H NMR (400 MHz, $CDCl_3$): δ (ppm) = 0.19 (s, 6H, CH_3), 0.98 (s, 9H, CH_3), 1.34 (m, 12H), 1.74 (m, 2H), 1.81 (m, 2H), 2.52 (t, J = 7.5 Hz, 2H), 4.00 (t, J = 6.5 Hz, 2H), 6.80 (d, J = 8.9 Hz, 2H), 6.90 (d, J = 8.9 Hz, 2H), 7.00 (d, J = 8.8 Hz, 2H), 7.53 (d, J = 8.8 Hz, 2H), 7.63 (d, J = 8.6 Hz, 2H), 7.68 (d, J = 8.6 Hz, 2H). ^{13}C NMR (100 MHz, $CDCl_3$): δ (ppm) = 24.9, 25.6, 26.0, 29.1, 29.2, 29.3, 29.5, 34.3, 68.1, 110.0, 115.1, 119.1, 120.5, 122.2, 127.0, 128.3, 131.2, 132.5, 144.7, 145.3, 153.1, 159.8, 172.5. FTIR (KBr, ν cm^{-1}): 2932, 2843, 2225, 1737, 1605, 1507, 1249. EA for $C_{36}H_{47}O_4NSi$: calc.: C 73.80, H 8.09, N 2.39; found: C 73.49, H 8.09, N 2.39%.

Compound 10. Compound **9** (1.47 g, 2.5 mmol) was dissolved in THF (15 mL) in a plastic vessel. Hydrofluoric acid (1.8 mL, 49% aqueous solution) was added by syringe and stirred. The reaction was diluted with dichloromethane and quenched with a saturated solution of sodium bicarbonate. The resultant mixture was washed several times with water and the crude product was purified by column chromatography using dichloromethane–ethyl acetate (10/0.2) as eluent. Yield: 0.54 g of a white solid (46%). M.p. (°C): 147. ^{1}H NMR (400 MHz, $CDCl_3$): δ (ppm) = 1.28 (m, 12H), 1.60 (m, 2H), 1.71 (m, 2H), 2.52 (t, J = 7.5 Hz, 2H), 4.00 (t, J = 6.5 Hz, 2H), 6.74 (d, J = 8.9 Hz, 2H), 6.86 (d, J = 8.9 Hz, 2H), 7.03 (d, J = 8.8 Hz, 2H), 7.68 (d, J = 8.2 Hz, 2H), 7.81 (d, J = 8.7 Hz, 2H), 7.84 (d, J = 8.6 Hz, 2H). ^{13}C NMR (100 MHz, $CDCl_3$): δ (ppm) = 24.2, 28.3, 228.5, 228.6, 33.3, 67.4, 108.9, 115.0, 118.8, 122.2, 126.6, 130.1, 132.6, 142.5, 144.1, 154.8, 159.2, 172.0. FTIR (KBr, ν cm^{-1}): 3259, 2929, 2840, 2220, 1739, 1604, 1502, 1246.

Compound BIPH. Acid **4** (0.40 g, 0.4 mmol), DMAP (0.04 g, 0.12 mmol), DCC (0.80 g, 0.4 mmol) and compound **10** (0.20 g, 0.40 mmol) were stirred in dry dichloromethane (50 mL) for 24 h. The crude product was purified by liquid chromatography on silica gel using dichloromethane as eluent. Compound **BIPH** was obtained as a white solid. Yield: 0.27 g (47%). M.p. (°C): see Table 1. ^{1}H NMR (400 MHz, $CDCl_3$): δ (ppm) = 0.89 (t, J = 6.6 Hz, 3H), 1.27 (m, 48H), 1.81 (m, 8H), 2.53 (t, J = 7.5 Hz, 2H), 2.56 (t, J = 7.5 Hz, 2H), 4.00 (t, J = 6.5 Hz, 2H), 4.06 (t, J = 6.5 Hz, 4H), 6.99 (d, J = 7.5 Hz, 6H), 7.08 (s, 4H), 7.23 (m, 1H), 7.30 (d, J = 8.6 Hz, 2H), 7.37 (d, J = 8.8 Hz, 2H), 7.39 (d, J = 8.8 Hz, 2H), 7.46 (m, 1H), 7.53 (m, 4H), 7.67 (m, 6H), 8.16 (d, J = 8.7 Hz, 4H), 8.30 (d, J = 8.1 Hz, 2H), 8.31 (d, J = 8.8 Hz, 2H). ^{13}C NMR (100 MHz, $CDCl_3$): δ (ppm) = 14.0, 22.6, 24.8, 25.9, 29.0, 29.1, 29.3, 29.5, 29.6, 31.8, 34.2, 68.0, 68.2, 68.1, 114.3, 115.0, 120.4, 122.0, 122.3, 124.6, 126.4, 127.0, 128.2, 129.9, 131.0, 131.7, 132.3, 137.9, 142.0, 145.2, 147.8, 150.1, 151.2, 155.6, 159.7, 163.7, 164.4, 172.1. FTIR (KBr, ν cm^{-1}): 2933, 2845, 2221, 1739, 1648, 1509, 1245. MALDI-MS m/z = 1523.9 $[M + Na]^+$. EA for $C_{95}H_{105}NO_{15}$: calc.: C 76.02, H 7.05, N 0.93; found: C 75.82, H 7.12, N 0.93%.

2. Experimental techniques

The textures of the mesophases were studied using an Olympus polarizing microscope equipped with a Linkam LTSE350 hot stage and a Linkam TMS-93 temperature controller. Photomicrographs were taken using an Olympus C-5050 camera on samples in Linkam cells (5 μm thick).

Heat capacity data at normal pressure were obtained by means of a commercial differential scanning calorimeter DSC-Q2000 from TA-Instruments working in modulated mode (MDSC). The experimental conditions were adjusted in such a way that the imaginary part of the complex heat capacity data vanished. Likewise, by means of a special calibration procedure in which very precise latent heat data measured from other homologous-compounds through adiabatic calorimetry are considered, the MDSC-technique is also suitable for quantitative measurements of latent heats of first order transitions, even if they are weak. A more detailed description of the MDSC technique can be found elsewhere.[16] The MDSC measurements were made as a standard study of the overall thermal behaviour of the samples and consisted of heating runs at 1 K min^{-1} from room temperature up to the I-phase and cooling runs at the same rate. In some cases, other slower rates were considered. The parameters of modulation (temperature amplitude and

oscillation period) were ±0.5 K and 60 s and the sample masses (chosen between 2 and 3 mg) were selected to ensure a uniform thin layer within the aluminium pans.

X-ray studies were performed on non-oriented samples in Debye–Scherrer geometry mode using Lindemann capillaries of diameter 0.6 mm. The materials were introduced by capillarity in the isotropic phase. Wide-angle measurements were carried out using a powder goniometer equipped with a high temperature attachment. A linear position-sensitive detector (PSD), with an angular resolution better than 0.01°, was employed to detect the diffracted intensity in the 2θ interval 0.5–25° (θ is the Bragg angle). A small-angle goniometer with a different temperature controller and a fixed position PSD of 4° of angular range was also employed. Monochromatic Cu-Kα radiation (λ = 1.5418 Å) was used in both cases.

Measurements of the complex dielectric permittivity $\varepsilon^*(f) = \varepsilon'(f) - i\varepsilon''(f)$, in the range of 10^3 to 1.1×10^8 Hz, were performed using an impedance analyzer (HP4294A). The cell consisted of two gold-plated brass electrodes (diameter 5 mm) separated by thick silica spacers of the order of 50 μm. A modified HP16091A coaxial test fixture was used as the sample holder. This was held in a cryostat from Novocontrol and both temperature and dielectric measurements were computer-controlled. Dielectric measurements were performed on cooling runs.

Results and discussion

Liquid crystal characterization

The mesomorphic properties of the dimers were investigated by polarizing optical microscopy (POM), modulated differential scanning calorimetry (MDSC), and X-ray diffraction (XRD). The transition temperatures and corresponding enthalpy values for the products are summarized in Table 1. Detailed explanations of the liquid crystalline behaviour listed in Table 1 are given below.

Two out of the three dimers form mesophases. Unfortunately, dimer **AZO1** did not show liquid crystalline properties and was not studied further. However, both hybrid bent-rod dimers containing a phenyl ring as the linker formed mesophases. Interestingly, in spite of the ability of both rigid cores to promote mesophase formation, a long and flexible spacer such as the one present in **AZO1** dramatically prevents the appearance of a soft-phase, in contrast to **AZO2**, which is based on the same bent- and rod-cores. Furthermore, the thermal behaviour of the two mesogenic dimers **AZO2** and **BIPH** is quite complex and it was studied in detail by different techniques.

Firstly, we will consider compound **AZO2**. The nature of the mesophases formed by this compound were assigned by both POM and XRD. On cooling from the isotropic liquid, a sample placed on 5 μm thick glass cells treated for parallel alignment showed a uniform birefringent texture that was characteristic of the nematic mesophase (Fig. 1a). On further cooling, a transition to a striped texture was observed at around 123 °C (Fig. 1b). This texture evolved to a fan-shaped texture that is characteristic of a SmA arrangement (Fig. 1c). The nematic nature (N) of the high temperature mesophase was confirmed by XRD experiments. Two diffuse halos, one in the low angle region and another in the wide angle one, were detected in the XR diffractogram, thus confirming the N character of the phase. However, it was not possible to study the low temperature phase by XRD as the sample crystallized during the experiment.

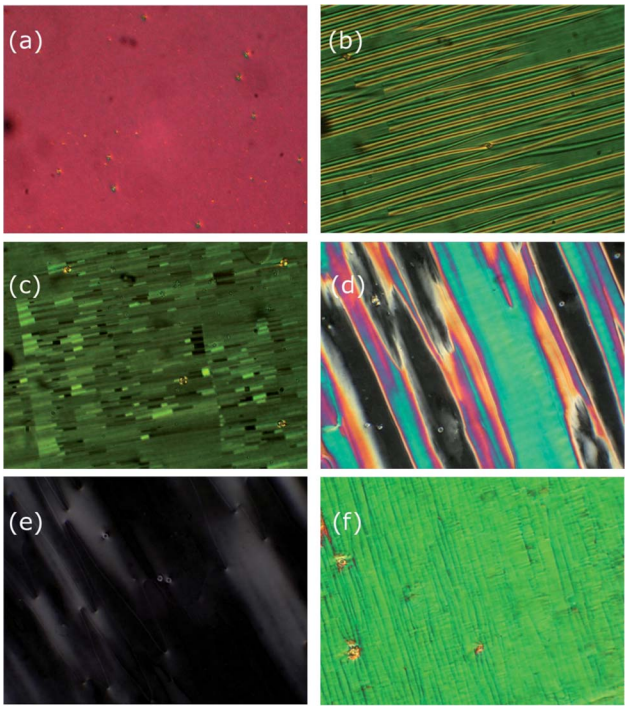

Fig. 1 Microphotographs of the textures observed for compound **AZO2** (a) at 139 °C in the N phase, (b) at 123 °C in the transition from the N to the M phase, (c) at 121 °C in the M phase, (d) at 121 °C under the application of a triangular wave-electric field of 20 V μm^{-1} and 50 Hz, (e) the same field conditions one minute later and (f) half a minute after removal of the field. The width of all photographs is about 300 μm and the rubbing direction is along the stripes.

In order to ascertain the nature of the lower temperature mesophase, its optical response to electric fields was studied (see Fig. 1c–f). Thin films of planar aligned **AZO2** (Linkam cells, 5 μm thick) could be switched from an optically transmitting state to a homeotropic black state. Dark lines developed in a direction perpendicular to the rubbing direction and spread over the whole sample. This behaviour is consistent with a positive dielectric anisotropy, which will be discussed later. In a relatively short period of time (30 seconds) after removal of the field, a quite homogenous planar texture was recovered. Such switching behaviour would not be expected in a SmA mesophase, where the transition in the texture is in general accompanied by the appearance of defects. This behaviour is more reminiscent of that found in other dimers for which a low temperature nematic mesophase is proposed, such as the twist-bend nematic phase.[1e,f] Unfortunately the narrow temperature range made it difficult to characterize this mesophase unambiguously and it will be denoted by the letter M.

Heat capacity data as a function of temperature were recorded in a heating run from the crystal (Cr) to isotropic liquid (I) phase for **AZO2** and a plot is shown in Fig. 2 (black symbols). The first heat capacity effect at lower temperatures shows a two-fold peak with a wide coexistence region of about 7 K. This type of effect is usually found in multiple phase transitions and in

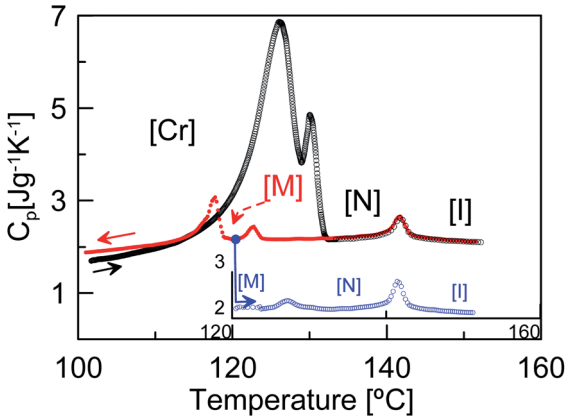

Fig. 2 Specific heat capacity data as a function of temperature for a sample of compound **AZO2**. Black and red symbols represent data collected on heating and cooling runs at 1 °C min^{-1}, respectively. Blue symbols correspond to a heating run from 120 °C after cooling from the isotropic phase without reaching crystallization.

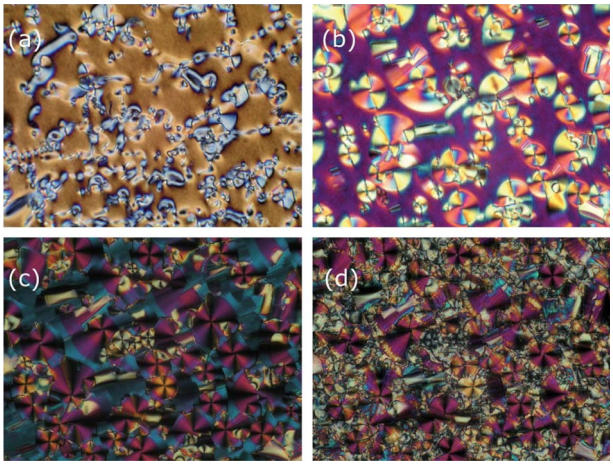

Fig. 3 Microphotographs of the textures of compound **BIPH**: (a) in the N phase at 136 °C, (b) in the N-SmX mesophase at 132 °C, (c) in the SmX at 124 °C, and (d) in the SmY phase at 123 °C. The width of the four photographs is about 300 μm.

this case seems to represent the Cr-to-M-to-N phase transition. On further heating another heat capacity peak is observed, which according to the POM information is attributed to the N-to-I phase transition. A subsequent cooling run from the liquid phase at the same rate is also represented in Fig. 2 (red symbols). The heat capacity peak corresponding to the I-to-N phase transition is observed at almost the same temperature as that in the heating run. At lower temperatures, two well-separated peaks are obtained and this indicates the appearance of another mesophase, which was identified as M according to our POM experiments. This phase sequence is fully reversible. Finally, on cooling the sample down to a temperature of about 120 °C (M mesophase) and then reheating it, the M-to-N transition could be observed clearly (blue symbols in the inset in Fig. 2) and both the temperature and latent heat could be calculated with a degree of accuracy.

Calculation of the latter parameter requires a special calibration and the following expression for the total enthalpy change associated with any transition (ΔH^{TOT}):

$$\Delta H^{TOT} = \Delta H + \int \Delta C_p dT \quad (1)$$

The second term on the right-hand side of eqn (1) is the pre-transitional fluctuation contribution (ΔC_p being the difference $C_p - C_{p,background}$ due to the change in orientational order intrinsic to this transition) and the latent heat is ΔH, which vanishes for second order transitions. In strongly first order phase transitions, the second term on the right-hand side of eqn (1) can be neglected due to the latent heat and the total enthalpy change is identified with the latent heat associated with the phase transition. This is the case for the latent heat associated with the two-fold peak attributed to the Cr-to-M-to-N phase transition. However, for the M-to-N and N-to-I transitions the second term on the right-hand side of eqn (1) must be taken into account in the calculation of the latent heats. The calculated values for compound **AZO2** are listed in Table 1 together with the corresponding transition temperatures.

We will now consider the other mesogenic dimer, *i.e.*, **BIPH**. On cooling from the isotropic phase, a characteristic texture of a nematic mesophase was observed for this material over a narrow temperature range. Almost simultaneously some circular and fan-shaped domains characteristic of smectic phases started to grow slowly as fractal nuclei, as shown in Fig. 3a. This coexistence of both mesophases extended over approximately 12 degrees (Fig. 3b). XRD experiments confirmed the nematic and lamellar character of the coexisting mesophases. The wide-angle diffraction patterns of **BIPH** at two temperatures in the coexistence range are shown in Fig. 4. A diffractogram characteristic of a nematic arrangement was recorded at 137 °C on cooling from the isotropic phase (orange symbols in Fig. 4). On further cooling, sharp peaks appeared that were superimposed on the nematic pattern and these became more intense on lowering temperature (the pattern in Fig. 4 shown in black points was obtained at 135 °C). The structure of this new mesophase was investigated using a low angle goniometer. The small angle diagrams observed for three different temperatures in a cooling run are shown in the inset in Fig. 4. Patterns in red and blue points correspond to temperatures within the coexistence region. These are indexed on the basis of a single periodicity of 87 Å. This value is significantly smaller than the theoretical molecular length (102 Å) calculated using Chemsketch. Given the resulting length of the combination of both spacers it is difficult to determine whether the molecules are bent within the layers or tilted and interdigitated in a similar way to that reported for Janus-dendrimer analogues.[14b] Hence, this mesophase will be denoted as SmX. Finally, at about 120 °C a change in the texture was observed and this corresponds to a transition to another phase (Fig. 3d). The small angle diffraction pattern observed below this temperature is virtually identical to those observed in the coexistence region (diagram with green points in the inset in Fig. 4). In fact, the structure presents the same periodicity as the SmX phase. However, the appearance of small peaks on the wide angle diffuse halo together with the dielectric behaviour, which

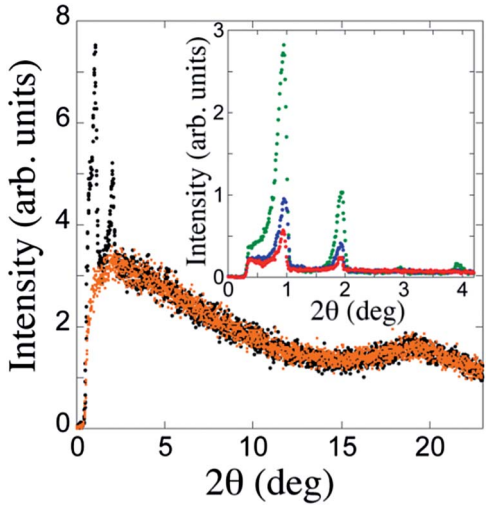

Fig. 4 Wide-angle X-ray diffraction patterns for compound **BIPH** at different temperatures in the phase coexistence range. The intensity is plotted as a function of 2θ, where θ is the Bragg angle. Orange points in the diagram are characteristic of a nematic structure (data at 137 °C). Black points in the diagram indicate that a lamellar phase grows within the nematic bulk (data at 135 °C). The inset represents the diffraction patterns obtained with a small-angle goniometer. Red and blue points correspond to the coexistence range as the temperature is lowered. Green points correspond to the low temperature phase (data at 120 °C). All the diagrams were indexed on the basis of a single periodicity.

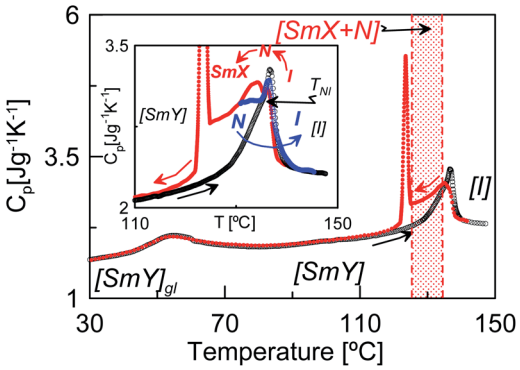

Fig. 5 Specific-heat data as a function of temperature for a sample of compound **BIPH**. Black and red symbols relate to data collected in heating and cooling runs at 1 °C min^{-1}, respectively. The inset shows the detail of the specific heat around both the SmX-to-N and the N-to-I phase transitions. Blue symbols correspond to a heating run on slow cooling at 0.5 °C min^{-1} from the I phase down to 134 °C. Coexistence regions are marked by shaded areas.

is discussed below, strongly suggests that in this phase the molecules have a higher degree of order. Consequently, hereafter this phase will be denoted as SmY. The switching response under electric fields was also investigated for **BIPH**. The effect of different fields on the region of the N-SmX phase coexistence is consistent with reorientation of the nematic phase towards a homeotropic dark state. In the present case, an electrooptic effect was not detected for the SmX and SmY phases, thus ruling out the possibility of polar order in the mesophases.

The phase sequence observed optically was confirmed by a careful analysis of the thermal behaviour. The heat capacity data for **BIPH** on cooling from the isotropic phase down to room temperature (red symbols) and on subsequent heating up to the isotropic phase (black symbols) are represented in Fig. 5. Three transitions can be identified on cooling from the isotropic phase. The first peak at higher temperatures warrants careful analysis. The inset in Fig. 5 shows the existence of a two-fold peak that, according to the textures, should correspond to the I-to-N and to the N-to-SmX phase transitions. The high heat capacity (red shaded region) is a sign of the coexistence of two phases, which were identified as the N and SmX mesophases. On further cooling to about 120 °C a transition was detected and this can be assigned to the SmX-to-SmY phase transition. Finally, the heat capacity effect at lower temperatures (about 45 °C) corresponds to a glass transition that provides evidence of the disordered character, at least from a dynamic point of view, of the SmY mesophase. In the subsequent heating experiment a similar glass transition was also observed and this was followed by a single broad peak at higher temperatures, which is assumed to be due to both the SmY-to-SmX and the N-to-I phase transitions, with SmX slowly evolving towards the N mesophase. An attempt to isolate the N–I transition was successful on slowly cooling the sample to 134 °C at 0.5 °C min^{-1}. On re-heating the sample a defined peak was obtained at about 135 °C. Temperatures and latent heats associated with the observed phase transitions are listed in Table 1.

Dielectric characterization

In order to gain further insights into the mesogenic behaviour of these two bent-core dimers, the temperature dependence of the dielectric permittivity at 1 kHz for both materials was determined in cooling runs from the isotropic phase (Fig. 6). Dielectric results for both compounds were obtained under two different dc bias field conditions (no field and an applied dc bias voltage of 0.8 V μm^{-1}). The transitions between the different mesophases described in the previous section can be envisaged as changes in the permittivity. Due to the reorientation of the important dipole moment of the cyano-groups of the two rod-like units, both materials show an increase in permittivity under field conditions. The static permittivity of the nematic phase of **AZO2** behaves in the same way as the nematic phase of rod-like liquid crystals, with $\Delta\varepsilon > 0$. In the case of **BIPH**, the dielectric anisotropy is smaller than in the case of **AZO2**, indicating that the coexistence of the nematic and lamellar mesophase hinders the reorientation of the rod-core unit under dc bias conditions. Furthermore, the slow decrease in the permittivity on decreasing the temperature coincides with the gradual transition from the N to the SmX phase. Finally, as can be observed in Fig. 6, the dielectric response of compound **BIPH** drops at the transition to the low temperature phase SmY, a finding that is consistent with a transition to a mesophase with a higher degree of order, as inferred from XRD studies.

The dynamic behaviour of the dimers was analysed by broadband dielectric spectroscopy measurements in the different mesophases as a function of temperature for both dimers. The temperature and frequency dependence of the

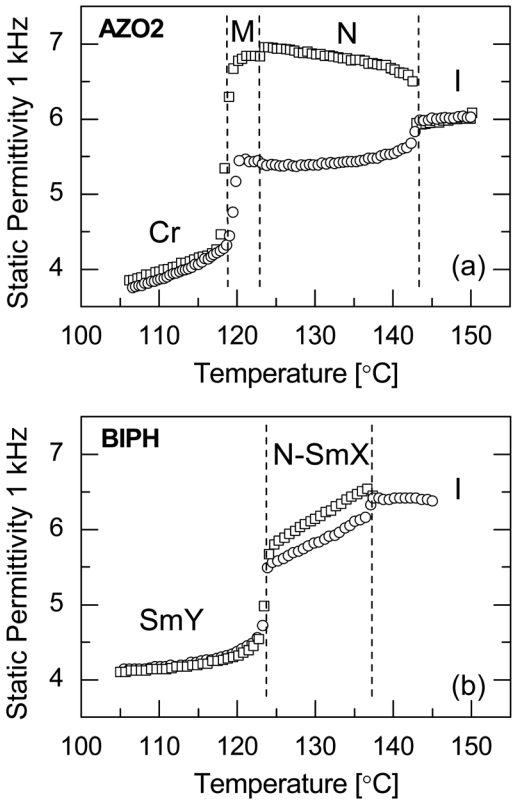

Fig. 6 Dielectric permittivity *versus* temperature for compound **AZO2** (top) and compound **BIPH** (bottom) in cooling runs.

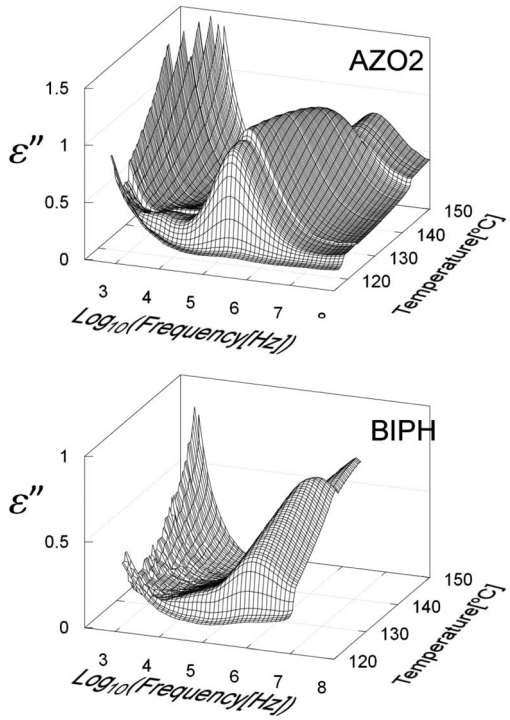

Fig. 7 Three-dimensional plot of dielectric losses *versus* temperature and the logarithm of the frequency for compounds **AZO2** (top) and **BIPH** (bottom) under 40 V dc bias field conditions.

imaginary part of the permittivity for **AZO2** and **BIPH** under field conditions are shown in the three-dimensional plots in Fig. 7. At first glance, the dielectric spectra shown in Fig. 7 do not seem to be complex. However, a closer inspection shows several relaxation processes that complicate the interpretation of the results. Both spectra seem to be dominated by a relaxation process whose frequency is around 1 MHz, indicating a low thermal activation. For **AZO2** the strength of this mode is independent of temperature but for **BIPH** it rapidly decreases on decreasing the temperature, *i.e.*, with the slow conversion of the nematic phase to the SmX phase.

In order to characterize the relaxation processes found, the dielectric permittivity can be expressed as a sum of all the possible contributions:

$$\varepsilon(\omega) = \sum_k \frac{\Delta\varepsilon_k}{\left[1 + (i\omega\tau_k)^{\alpha_k}\right]^{\beta_k}} + \varepsilon_\infty - i\frac{\sigma_{dc}}{\varepsilon_0\omega} \qquad (2)$$

where $\Delta\varepsilon_k$ is the dielectric strength of each relaxation mode, τ_k the relaxation time related to the frequency of maximum dielectric loss, α_k and β_k are parameters that describe the shape (symmetry and width) of the relaxation spectra ($\alpha_k = \beta_k = 1$ corresponds to Debye relaxation) and σ_{dc} is the dc conductivity. The summation is extended over all relaxation modes, and each one is fitted according to the Havriliak–Negami (H–N) function.

As an example, the two components of the complex dielectric permittivity under two different dc bias conditions for **AZO2** at 125 °C in the nematic phase are shown in Fig. 8. The dielectric relaxation curves show different distinguishable relaxation processes and this provides evidence that both the bent-core

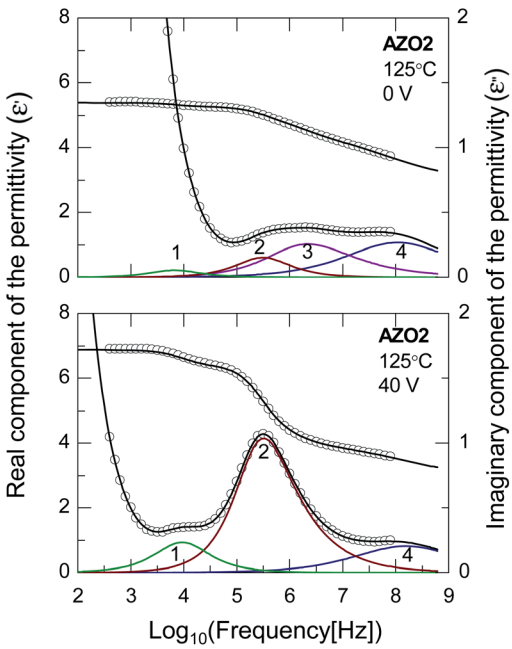

Fig. 8 Frequency dependence of the dielectric permittivity of compound **AZO2** in the N phase (T = 125 °C), with no field (top) and with a dc bias field of 40 V (bottom). Black solid lines are fittings according to eqn (2) and coloured lines represent the deconvolution into elementary modes.

and the rod-unit contribute to the dielectric permittivity. The assignment of each contribution to the corresponding molecular or intramolecular reorientation is not straightforward. Due to the cumulative length of the flexible spacer between the bent-core and the rod-like moieties, it seems reasonable to consider that both groups reorient independently. Under this assumption, the frequency of the process denoted as 2 in the graphs and the increase in its strength under field conditions allow us to attribute this mode to the reorientation of the rod-like units, *i.e.*, the reorientation of the unit containing the cyano-group. This mode shows an almost constant strength over the whole temperature range, with a value of 2.7 in the nematic mesophase and 2.5 in the M mesophase and an activation energy of 109 kJ mol^{-1}. The identification of all the different relaxation processes requires further data and is beyond the scope of the present work. In the case of **BIPH**, such analysis is even more difficult since the effect of electric fields is weak due to the phase coexistence.

Concluding remarks

Novel non-symmetric dimers, whose molecular design is based on a promesogenic bent-shaped structure joined to two different promesogenic rod-like moieties derived from cyanobiphenyl and azobenzene units, have been synthesized. In contrast to previous reports, and with the aim of decoupling the rigid cores, very long spacers (two chains of 10 methylene units), linked either by a phenyl ring or a hexamethylene-triazole moiety, have been used. Interestingly, the use of the latter linkage prevented the appearance of mesomorphism. However, in the former two cases these unusually long spacers have proven to be suitable to promote mesophases with a complex nature. It was also found that the structure of the rod-like unit strongly affects the final mesophases exhibited by the materials. Thus, for the dimer containing a cyanobiphenyl rod-like unit (**BIPH**), an unstable nematic mesophase is formed and this evolved to a lamellar SmX and then to the non-polar SmY mesophase. However, in the case of the azobenzene-based dimer (**AZO2**) the –N=N– linking group increases the length and polarizability. It confers a core structure in which linearity is maintained, but the broadness tends to disrupt a lamellar order thus enabling the formation of the nematic mesophase, as it is commonly reported for azobenzene based liquid crystals.[17] A dielectric study of these materials revealed a complex dynamic behaviour. Due to the cumulative length of the linking group, the reorientational dynamics of the bent-core system and the rod-like units are significantly different. Furthermore, it was shown that the strong dipole moment associated with the cyano-group allows the reorientation of the alignment by the application of strong electric fields.

Acknowledgements

The authors greatly appreciate financial support from the Spanish Government (MICINN-FEDER project MAT2009-14636-C03 and MINECO-FEDER projects MAT2012-38538-C03-01/02/03 and CTQ2012-35692), the Aragon-FSE (project E04) and Basque (GI/IT-449-10) Governments, and the recognition from the Generalitat de Catalunya of GRPFM as Emergent Research Group (2009-SGR-1243). The authors are also grateful to the JAE-DOC-CSIC program (N. Gimeno), the Universidad del País Vasco for a post-doctoral grant (N. Sebastián) and to the BSCH-UZ and GA (project E04) (J. Vergara) fellowship program for support. Thanks are also given to Nuclear Magnetic Resonance, Mass Spectroscopy and Thermal Analysis Services from the CEQMA, Universidad de Zaragoza–CSIC (Spain).

References

1 (*a*) C. T. Imrie, *Liq. Cryst.*, 2006, **33**, 1449; (*b*) C. T. Imrie and P. A. Henderson, *Curr. Opin. Colloid Interface Sci.*, 2002, **7**, 298; (*c*) C. T. Imrie and P. A. Henderson, *Chem. Soc. Rev.*, 2007, **36**, 2096; (*d*) C. T. Imrie, P. A. Henderson and G. Y. Yeap, *Liq. Cryst.*, 2009, **36**, 755; (*e*) M. Cestari, S. Diez-Berart, D. A. Dunmur, A. Ferrarini, M. R. de la Fuente, D. J. B. Jackson, D. O. López, G. R. Luckhurst, M. A. Pérez-Jubindo, R. M. Richardson, J. Salud, B. A. Timimi and H. Zimmerman, *Phys. Rev. E: Stat., Nonlinear, Soft Matter Phys.*, 2011, **84**, 031704; (*f*) V. Borshch, Y.-K. Kim, J. Xiang, M. Gao, A. Jákli, V. P. Panov, J. K. Vij, C. T. Imrie, M. G. Tamba, G. H. Mehl and O. D. Lavrentovich, *Nat. Commun.*, 2013, **4**, DOI: 10.1038/ncomms3635.

2 S. Kumar, *Liq. Cryst.*, 2005, **32**, 1089.

3 T. Niori, *J. Mater. Chem.*, 1996, **6**, 1231.

4 (*a*) G. Pelzl, S. Diele and W. Weissflog, *Adv. Mater.*, 1999, **11**, 707; (*b*) D. M. Walba, *Topics in Stereochemistry, Materials-Chirality*, 2003, vol. 24, p. 457; (*c*) C. Tschierske and G. Dantlgraber, *Pramana*, 2003, **61**, 455; (*d*) M. B. Ros, J. L. Serrano, M. R. De La Fuente and C. L. Folcia, *J. Mater. Chem.*, 2005, **15**, 5093; (*e*) W. Weissflog, H. N. Shreenivasa Murthy, S. Diele and G. Pelzl, *Philos. Trans. R. Soc., A*, 2006, **364**, 2657; (*f*) R. A. Reddy and C. Tschierske, *J. Mater. Chem.*, 2006, **16**, 907; (*g*) C. Pelzl, W. Weissflog, *Thermotropic Liquid Crystals: Recent Advances*, 2007, vol. 1, p. 1.

5 (*a*) J. Etxebarria and M. B. Ros, *J. Mater. Chem.*, 2008, **18**, 2919; (*b*) A. Jákli, I. C. Pintre, J. L. Serrano, M. B. Ros and M. R. De La Fuente, *Adv. Mater.*, 2009, **21**, 3784; (*c*) I. C. Pintre, J. L. Serrano, M. B. Ros, J. Martínez-Perdiguero, I. Alonso, J. Ortega, C. L. Folcia, J. Etxebarria, R. Alicante and B. Villacampa, *J. Mater. Chem.*, 2010, **20**, 2965; (*d*) J. Harden, M. Chambers, R. Verduzco, P. Luchette, J. T. Gleeson, S. Sprunt and A. Jákli, *Appl. Phys. Lett.*, 2010, **96**, 102907; (*e*) A. Eremin and A. Jákli, *Soft Matter*, 2013, **9**, 615.

6 (*a*) G. R. Luckhurst, *Thin Solid Films*, 2001, **393**, 40; (*b*) C. Tschierske, *Curr. Opin. Colloid Interface Sci.*, 2002, **7**, 69; (*c*) B. Acharya, A. Primak, T. J. Dingemans, E. T. Samulski and S. Kumar, *Pramana*, 2003, **61**, 231; (*d*) M. A. Bates and G. R. Luckhurst, *Phys. Rev. E: Stat., Nonlinear, Soft Matter Phys.*, 2005, **72**, 051702; (*e*) B. Mettout, *Phys. Rev. E: Stat., Nonlinear, Soft Matter Phys.*, 2005, **72**, 031702.

7 (*a*) H. Takezoe and Y. Takanishi, *Jpn. J. Appl. Phys., Part 1*, 2006, **45**, 597; (*b*) C. Keith, A. Lehmann, U. Baumeister, M. Prehm and C. Tschierske, *Soft Matter*, 2010, **6**, 1704; (*c*) C. Tschierske and D. J. Photinos, *J. Mater. Chem.*, 2010, **20**, 4263; (*d*) P. Grzybowski and L. Longa, *Phys. Rev. Lett.*, 2011,

107, 027802; (*e*) M. Lehmann, *Liq. Cryst.*, 2011, **38**, 1389; (*f*) M. Mathews, S. Kang, S. Kumar and Q. Li, *Liq. Cryst.*, 2011, **38**, 31; (*g*) J. Seltmann, K. Müller, S. Klein and M. Lehmann, *Chem. Commun.*, 2011, **47**, 6680.

8 C. V. Yelamaggad, S. Krishna Prasad, G. G. Nair, I. S. Shashikala, D. S. Shankar Rao, C. V. Lobo and S. Chandrasekhar, *Angew. Chem., Int. Ed.*, 2004, **43**, 3429.

9 G. Lee, H. Jeong, F. Araoka, K. Ishikawa, J. G. Lee, K. T. Kang, M. Cepic and H. Takezoe, *Liq. Cryst.*, 2010, **37**, 883.

10 Y. Wang, H. G. Yoon, H. K. Bisoyi, S. Kumar and Q. Li, *J. Mater. Chem.*, 2012, **22**, 20363.

11 (*a*) C. V. Yelamaggad, I. S. Shashikala, G. Liao, D. S. Shankar Rao, S. K. Prasad, Q. Li and A. Jakli, *Chem. Mater.*, 2006, **18**, 6100; (*b*) C. V. Yelamaggad, N. L. Bonde, A. S. Achalkumar, D. S. Shankar Rao, S. K. Prasad and A. K. Prajapati, *Chem. Mater.*, 2007, **19**, 2463.

12 (*a*) N. G. Nagaveni, V. Prasad and A. Roy, *Liq. Cryst.*, 2013, **40**, 1001; (*b*) M.-G. Tamba, A. Bobrovsky, V. Shibaev, G. Pelzl, U. Baumeister and W. Weissflog, *Liq. Cryst.*, 2011, **38**, 1531.

13 (*a*) M. G. Tamba, B. Kosata, K. Pelz, S. Diele, G. Pelzl, Z. Vakhovskaya, H. Kresse and W. Weissflog, *Soft Matter*, 2006, **2**, 60; (*b*) M. G. Tamba, U. Baumeister, G. Pelzl and W. Weissflog, *Liq. Cryst.*, 2010, **37**, 853.

14 (*a*) I. Giner, I. Gascon, J. Vergara, M. C. Lopez, M. B. Ros and F. M. Royo, *Langmuir*, 2009, **25**, 12332; (*b*) N. Gimeno, J. Vergara, M. Cano, J. L. Serrano, M. B. Ros, J. Ortega, C. L. Folcia, S. Rodríguez-Conde, G. Sanz-Enguita and J. Etxebarria, *Chem. Mater.*, 2013, **25**, 286.

15 (*a*) M. E. Neubert, S. S. Keast, J. M. Kim, A. G. Norton, M. J. Whyde, M. J. Smith, R. M. Stayshich, M. E. Walsh and D. G. Abdallah Jr, *Liq. Cryst.*, 2005, **32**, 347; (*b*) J. Del Barrio, L. Oriol, C. Sánchez, J. L. Serrano, A. Di Cicco, P. Keller and M. H. Li, *J. Am. Chem. Soc.*, 2010, **132**, 3762.

16 M. B. Sied, J. Salud, D. O. López, M. Barrio and J. Ll. Tamarit, *Phys. Chem. Chem. Phys.*, 2002, **4**, 2587.

17 *Flüssige Kristalle in Tabellen II*, ed. D. Demus and H. Zaschke, VeB Deutscher Verlag Für Grundstoffindustrie, Leipzig, 1984.

